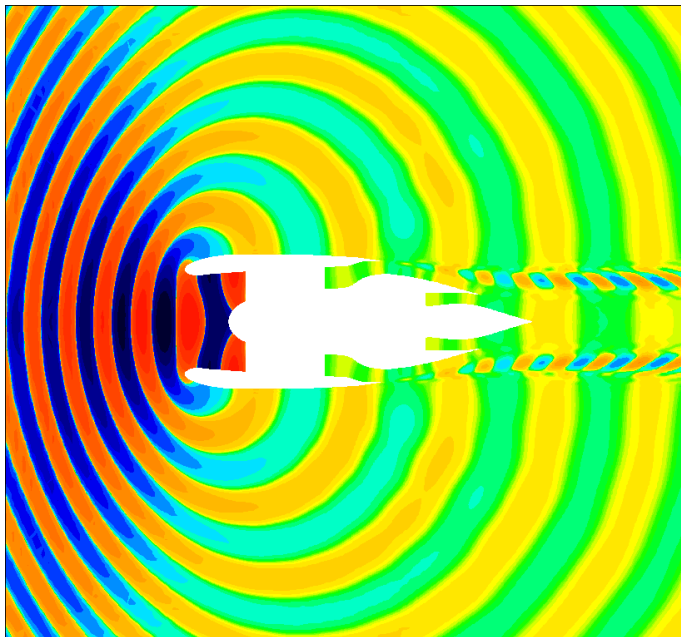




Executive Summary

A symmetry and dispersion-relation preserving high-order scheme for aeroacoustics and aerodynamics



Problem area

As the air transportation market grows, the noise generated by aircraft is increasingly becoming a serious environmental problem. Consequently, there is a need for new concepts and technologies that reduce the noise levels of future aircraft. The design of such low-noise aircraft can be supported by computational methods to analyze the generation and propagation of sound. For aircraft, sound is generated by the engines and also by the airframe, for example, due to the turbulent, massively separated flow induced by the landing gears.

Such flows can be computed using so-called extra-large eddy simulations (X-LES). Before the sound reaches the ground, it must travel through the non-uniform flow field surrounding the aircraft where its direction may change. The propagation of sound through a non-uniform flow can be computed using the linearized Euler equations.

Description of work

In order to compute the massively separated flows and the propagation of sound with sufficient accuracy, a high-order numerical scheme is presented in this report. This scheme

Report no.

NLR-TP-2006-525

Author(s)

J.C. Kok

Classification report

Unclassified

Date

August 2006

Knowledge area(s)

Computational Physics & Theoretical Aerodynamics

Descriptor(s)

High-order discretization
 Skew-symmetric form
 Dispersion-relation preserving
 Computational aeroacoustics
 Compressible turbulence
 Large-eddy simulation

prevents non-physical dissipation of the turbulent flow structures within the separated flows. It also ensures that sound is not dispersed or dissipated as it travels over long distances. Furthermore, the scheme preserves essential conservation and symmetry properties of the equations that are solved. Finally, the scheme is unique in that its high accuracy is maintained on smooth, non-uniform, curvilinear grids.

Results and conclusions

The high-order numerical scheme is applied to a number of basic test cases: the propagation of an acoustic pulse, the convection of an isentropic vortex, and the decay of isotropic, homogeneous turbulence. These cases clearly show the high

accuracy of the scheme, in particular on non-uniform, curvilinear grids. Furthermore, the numerical stability has been enhanced by the symmetry properties of the scheme.

Applicability

Extra-large eddy simulations are used to compute turbulent, massively separated flow. They can be applied, for example, to analyze the sound generation for landing gears, engine jets, and weapon bays. The linearized Euler equations are solved to compute the propagation of sound in a non-uniform flow. This can be applied, for example, to determine the far-field directivity and intensity of tonal sound generated by turbine fans or propellers.



NLR-TP-2006-525

A symmetry and dispersion-relation preserving high-order scheme for aeroacoustics and aerodynamics

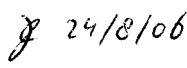

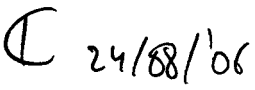
J.C. Kok

This report is based on a presentation to be held at ECCOMAS CFD 2006, Egmond aan Zee, The Netherlands, 5–8 September 2006.

This report may be cited on condition that full credit is given to NLR and the authors.

Customer National Aerospace Laboratory NLR
Contract number ----
Owner National Aerospace Laboratory NLR
Division Aerospace Vehicles
Distribution Unlimited
Classification of title Unclassified
 August 2006

Approved by:

Author	Reviewer	Managing department
 24/8/06	 24/8/06	 24/8/06

Summary

A new high-order, finite-volume scheme is presented that preserves the symmetry property and the dispersion relation of the convective operator. The scheme is applied to large-eddy simulation of compressible, turbulent flow and to the solution of the linearized Euler equations for aeroacoustic applications. For large-eddy simulation, the discretization is based on the skew-symmetric form, which ensures that the kinetic energy is conserved by the convective operator. This property minimizes the interference of numerical errors with the subgrid-scale model and also enhances numerical stability. Low numerical dispersion is obtained by extending the dispersion-relation preserving scheme of Tam & Webb to finite-volume schemes. The proposed finite-volume scheme is unique in that it is truly fourth-order accurate, conservative, symmetry preserving and dispersion-relation preserving on non-uniform, curvilinear structured grids.

Contents

List of figures	7
1 Introduction	9
2 Symmetry and conservation for compressible flow	10
3 Conservative discretization	12
4 Fourth-order discretization on curvilinear grids	14
5 Dispersion-relation preserving scheme on curvilinear grids	15
6 Propagation of an acoustic pulse	17
7 Convection of an isentropic vortex	19
8 Decaying isotropic homogeneous turbulence	23
9 Concluding remarks	25
Acknowledgements	25
References	26

8 Figures

(26 pages in total)

List of figures

Figure 1	Control volumes $\Omega_{i,j}^h$ and $\Omega_{i,j}^{3h}$ around cell centre (i, j) in 2D.	14
Figure 2	Numerical solution of 2D acoustic pulse at time $ct/L = 32$ on strongly non-uniform curvilinear grid with 200×200 grid cells	18
Figure 3	Numerical solution of 2D acoustic pulse at time $ct/L = 32$ on strongly non-uniform curvilinear grid with varying number of grid cells compared to analytic solution at $y = 0$	19
Figure 4	Convection of strong isentropic vortex on strongly non-uniform grid: temperature field at time $u_\infty t/L = 150$ (centre should be located at $(x, y) = (75L, 0)$) on medium grid (200×200 cells)	21
Figure 5	Convection of strong isentropic vortex on strongly non-uniform grid: Grid dependence of root-mean-square value of difference with analytical solution at time $u_\infty t/L = 150$	22
Figure 6	Compressible isotropic homogeneous turbulence: time dependence of total kinetic energy for inviscid computations with low-dispersion fourth-order scheme using skew-symmetric and divergence forms and without artificial diffusion	24
Figure 7	Incompressible isotropic homogeneous turbulence: grid dependence of energy spectra for second-order and low-dispersion fourth-order schemes	24
Figure 8	Incompressible isotropic homogeneous turbulence: decay of total kinetic energy for low-dispersion fourth-order scheme with and without sixth-order artificial diffusion	25



This page is intentionally left blank.

1 Introduction

As the air transportation market grows, the noise generated by aircraft is increasingly becoming a serious environmental problem. Consequently, there is a need for new concepts and technologies that reduce the noise levels of future aircraft. The design of such low-noise aircraft can be supported by computational methods to analyze the generation and propagation of sound. When the sound generation is related to turbulent, massively separated flow, such as the flow around a landing gear, then large-eddy simulations (LES) can be used, for example, to evaluate the effect on the sound level of geometric modifications. For full-scale Reynolds numbers, LES is still out of reach, but hybrid RANS–LES methods, such as extra-large eddy simulation (X-LES) (Ref. 4), are becoming feasible. Other examples of sound generation where X-LES may be useful are engine jets and weapon bays. A different approach in the field of computational aeroacoustics is the solution of the linearized Euler equations (LEE). With these equations, the propagation of sound in a non-uniform flow can be computed. This can be used, for example, to determine the far-field directivity and intensity of tonal sound generated by turbine fans or propellers.

The X-LES method and the linearized Euler equations have been implemented in a compressible, multi-block flow solver. This solver has been well-validated for applications based on the Reynolds-averaged Navier–Stokes equations. For such applications, second-order accuracy is sufficient. Large-eddy simulations, however, require a high-order discretization of the convective operator to avoid interference with the sub-grid scale model (see, e.g., Kravchenko & Moin (Ref. 6)). Also, solving the linearized Euler equations requires a high-order discretization to avoid excessive dispersion and dissipation of the sound waves as they travel over long distances. Therefore, the existing second-order, cell-centred, finite-volume scheme (Ref. 5) has been extended with a high-order numerical discretization of the convective terms.

The proposed numerical method is unique in that the following properties are truly maintained on smooth, non-uniform, curvilinear grids:

- fourth-order accuracy,
- conservation of mass, momentum, and total energy,
- conservation of kinetic energy by the convective operator,
- low numerical dispersion,
- no numerical dissipation, unless explicitly added.

The finite-volume method is made fourth-order accurate following the approach of Verstappen & Veldman (Refs. 8, 9) using Richardson extrapolation. They used this approach on Cartesian grids; here, it will be shown that this approach works for curvilinear grids as well. Minimization

of the dispersion of the numerical scheme is done following the so-called dispersion-relation preserving (DRP) approach of Tam & Webb (Ref. 7). It will be shown how the DRP approach can be combined with a conservative, finite-volume scheme. Finally, for turbulent flows, conservation of kinetic energy by the convective operator is obtained if the discretization is based on the skew-symmetric form. Verstappen & Veldman applied this so-called symmetry preserving approach to incompressible flow, for which it means that the total kinetic energy cannot increase (but only be dissipated by viscosity), so that numerical stability is ensured. For compressible flows, however, compression or expansion of the fluid results in an isentropic exchange of kinetic and internal energy (through work done by the pressure), allowing for an increase (as well as decrease) of total kinetic energy. Nevertheless, the skew-symmetric form ensures that the discretization of the convective operator does not interfere with the dissipation of kinetic energy due to viscosity or due to the sub-grid scale model in case of LES. It also enhances numerical stability, as will be shown here. For compressible flow, Feiereisen et al. (Ref. 2) were the first to present a skew-symmetric form and to show how it can be preserved for a finite-differencing scheme; here, it will be shown how it can be preserved for a finite-volume scheme.

2 Symmetry and conservation for compressible flow

A numerical method for the compressible Navier–Stokes equations will be presented that not only preserves the conservation of mass, momentum, and total energy, but also the conservation of kinetic energy by the convective operator. For this purpose, appropriate forms of the convective operator are defined in this section. For incompressible flow, it is well known that kinetic energy can be conserved if the discretization of the momentum equation is based on the skew-symmetric form. For compressible flow, the same can be done if the skew-symmetric form is defined appropriately.

The Navier–Stokes equations for a compressible flow are based on the conservation laws for mass, momentum, and total energy. If the equations are cast in divergence form, then integration of the equations over the flow domain and applying Gauss’ theorem shows that the total amount of mass, momentum, and energy cannot change (given appropriate boundary conditions). Hence, the divergence form expresses conservation.

An equation for the kinetic energy can be derived from the momentum equation. This equation cannot be cast into divergence form, because the kinetic energy of a compressible flow is not conserved. In particular, kinetic energy is dissipated by viscosity. Furthermore, work done by the pressure leads to an isentropic exchange of kinetic and internal energy in case of compression or

expansion of the fluid. The convection of kinetic energy, however, is conservative and therefore can be cast into divergence form. This divergence form follows immediately from the momentum equation if one uses the so-called skew-symmetric operator.

Convection of a physical quantity, like mass, momentum, and energy, can be described by several differential operators. The divergence form of the operator, expressing conservation, is given by

$$D\phi = \frac{\partial \rho \phi}{\partial t} + \nabla \cdot (\rho \mathbf{u} \phi), \quad (1)$$

with $\phi(t, \mathbf{x})$ the convected physical quantity per unit mass, ρ the density and \mathbf{u} the fluid velocity.

The advective operator,

$$A\phi = \rho \frac{\partial \phi}{\partial t} + \rho \mathbf{u} \cdot \nabla \phi, \quad (2)$$

gives the time derivative of ϕ while moving along with a fluid particle (multiplied by density).

The two forms are easily shown to be equivalent using the continuity equation for a compressible flow,

$$\frac{\partial \rho}{\partial t} + \nabla \cdot (\rho \mathbf{u}) = 0, \quad (3)$$

which expresses mass conservation (and is obtained by setting $\phi = 1$ in $D\phi = 0$).

Convection of a physical quantity implies conservation not only of the quantity itself, but also of its quadratic form (ϕ^2). This is expressed by the divergence operator applied to the quadratic form, which is derived by multiplying equations (1) and (2) with ϕ and applying the chain rule:

$$\phi D\phi + \phi A\phi = D(\phi^2). \quad (4)$$

In fact, a more general relation holds,

$$\phi D\theta + \theta A\phi = D(\phi\theta), \quad (5)$$

which means that D and $-A$ are adjoint operators. A symmetric (or self-adjoint) and a skew-symmetric operator are then naturally defined as $S = \frac{1}{2}(D - A)$ and $K = \frac{1}{2}(D + A)$, respectively, so that $D = K + S$ and $A = K - S$. The skew-symmetric operator has the property

$$\phi K\phi = D\left(\frac{1}{2}\phi^2\right), \quad (6)$$

which shows that using the skew-symmetric operator leads immediately to conservation of the quadratic form. Substituting the definitions of D and A , the symmetric and skew-symmetric operators are found to be

$$S\phi = \frac{1}{2} \left(\frac{\partial \rho}{\partial t} + \nabla \cdot (\rho \mathbf{u}) \right) \phi, \quad (7a)$$

$$K\phi = \frac{1}{2} \frac{\partial \rho \phi}{\partial t} + \frac{1}{2} \rho \frac{\partial \phi}{\partial t} + \frac{1}{2} \nabla \cdot (\rho \mathbf{u} \phi) + \frac{1}{2} \rho \mathbf{u} \cdot \nabla \phi. \quad (7b)$$

Note that it follows from the continuity equation that the symmetric operator is identical to zero, and that therefore the divergence, advective, and skew-symmetric operators are all equivalent.

Two alternatives for the skew-symmetric form for compressible flow can be found in the literature. Feiereisen et al. (Refs. 2, 3) use

$$\frac{\partial \rho \phi}{\partial t} + \frac{1}{2} \nabla \cdot (\rho \mathbf{u} \phi) + \frac{1}{2} \rho \mathbf{u} \cdot \nabla \phi + \frac{1}{2} \phi \nabla \cdot (\rho \mathbf{u}), \quad (8)$$

which is, in fact, the divergence operator, written as the sum of the skew-symmetric and symmetric operators (except for the time derivative). Others write the divergence operator as

$$\frac{\partial \rho \phi}{\partial t} + \frac{1}{2} \nabla \cdot (\mathbf{u} \rho \phi) + \frac{1}{2} \mathbf{u} \cdot \nabla (\rho \phi) + \frac{1}{2} \rho \phi \nabla \cdot \mathbf{u}, \quad (9)$$

but discretizations based on this form will not lead to conservation of ϕ^2 . This form seems to be based on the intuitive idea that $\rho \phi$ is the conserved quantity that is convected by the velocity \mathbf{u} . Convection, however, conserves the physical quantities of a fluid particle. As a fluid particle has a constant mass, and not a constant volume, the quantities per unit mass are conserved (ϕ) and not the quantities per unit volume ($\rho \phi$).

3 Conservative discretization

As stated above, the aim is to discretize the convective operator such that both momentum and kinetic energy are conserved. A finite-volume discretization of the flow equations, which is based on the divergence form, ensures conservation of mass, momentum, and total energy. To ensure conservation of kinetic energy, equation (6) should also hold in a discrete sense.

A finite-volume discretization of the gradient operator ∇F can be written as

$$\nabla_i F = \frac{1}{V_i} \sum_f F_f \mathbf{A}_f, \quad (10)$$

with V_i the volume of a grid cell Ω_i , F_f the flux at cell face f , and \mathbf{A}_f the area vector of cell face f . For a structured grid, the grid cells are numbered by a triple index $\mathbf{i} = (i, j, k)$ and the variables located at the cell centres are indicated with a subscript \mathbf{i} . The summation takes place over all faces f of the considered grid cell. Conservation requires that the fluxes at the cell faces are unique and that the area vectors satisfy the geometric conservation law

$$\sum_f \mathbf{A}_f = 0. \quad (11)$$

For a second-order central scheme, the fluxes are obtained by averaging the variables from the adjacent cells. When a flux consists of the product of several variables, one has to choose which variables are averaged. For this purpose, define the following averages

$$\bar{u}_f = \frac{1}{2}(u_{i,j,k} + u_{i+1,j,k}), \quad (12a)$$

$$\widetilde{uv}_f = \frac{1}{2}(u_{i,j,k}v_{i+1,j,k} + u_{i+1,j,k}v_{i,j,k}), \quad (12b)$$

where, without loss of generality, the face between cells $\Omega_{i,j,k}$ and $\Omega_{i+1,j,k}$ is considered. Now, using the geometric conservation law, the following rules can be derived for the discrete gradient operator,

$$\nabla_i \bar{u}\bar{v} = \frac{1}{2}\nabla_i \bar{u}\bar{v} + \frac{1}{2}\nabla_i \widetilde{uv}, \quad (13a)$$

$$\nabla_i \widetilde{uv} = u_i \nabla_i \bar{v} + v_i \nabla_i \bar{u}. \quad (13b)$$

In order to preserve equation (6) in a discrete sense, discretize the skew-symmetric operator as

$$K_i \phi = \frac{1}{2} \frac{d\rho_i \phi_i}{dt} + \frac{1}{2} \rho_i \frac{d\phi_i}{dt} + \frac{1}{2} \nabla_i \cdot \overline{\rho \mathbf{u} \phi} + \frac{1}{2} \rho_i \mathbf{u}_i \cdot \nabla_i \bar{\phi}. \quad (14)$$

Using the rules of equation (13), it is then possible to show that indeed

$$\phi_i K_i \phi = \frac{d}{dt} (\rho_i \frac{1}{2} \phi_i^2) + \nabla_i \cdot (\overline{\rho \mathbf{u}} \frac{1}{2} \phi \phi), \quad (15)$$

which is a finite-volume discretization of the divergence operator applied to ϕ^2 , ensuring conservation of ϕ^2 . Since equation (14) is not a finite-volume discretization of convection, the question remains whether ϕ itself is conserved. To this end, define the discrete divergence operator as $D_i = K_i + S_i$, with the symmetric operator discretized as

$$S_i \phi = \frac{1}{2} \left(\frac{d\rho_i}{dt} + \nabla_i \cdot \overline{\rho \mathbf{u}} \right) \phi_i. \quad (16)$$

Using again the rules of equation (13), one finds that

$$D_i \phi = \frac{d\rho_i \phi_i}{dt} + \nabla_i \cdot \overline{\rho \mathbf{u} \phi}, \quad (17)$$

which is indeed a finite-volume discretization of the divergence operator applied to ϕ . Thus, both ϕ and ϕ^2 are conserved.

Finally, a second-order finite-volume discretization of convection that conserves both momentum and kinetic energy is obtained by discretizing the continuity equation according to equation (16), by applying equation (17) to the convective term in the momentum equation, and by applying equation (15) to the convective term of the kinetic energy equation (as part of the total energy equation).

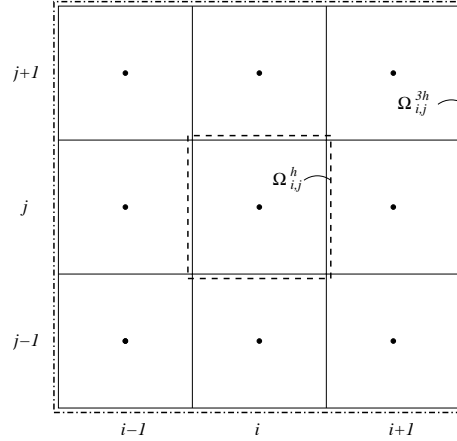


Fig. 1 Control volumes $\Omega_{i,j}^h$ and $\Omega_{i,j}^{3h}$ around cell centre (i, j) in 2D.

4 Fourth-order discretization on curvilinear grids

The second-order discretization of the previous section is extended to fourth order by Richardson extrapolation. Consider the second-order scheme for the gradient operator in \mathbb{R}^d , written as

$$V_i^h \nabla_i F = B_i^h, \quad (18)$$

with the flux balance B_i^h given by

$$B_i^h = \sum_f F_f^h A_f^h, \quad (19)$$

and with the superscript h indicating the mesh size in the computational domain. Also consider an additional second-order schemes consisting of the same discretization stencil applied on a grid with a three times larger mesh size in the computational domain (indicated with superscripts $3h$). For each cell centre, the control volume Ω^{3h} of the $3h$ scheme is constructed by joining the 3^d cells around the cell centre, as illustrated in figure 1 in 2D. This discretization of the gradient operator can be written as

$$V_i^{3h} \nabla_i F = B_i^{3h}, \quad (20)$$

with V_i^{3h} the volume of the control volume Ω_i^{3h} and with the flux balance B_i^{3h} given by

$$B_i^{3h} = \sum_f F_f^{3h} A_f^{3h}, \quad (21)$$

where the summation takes places over the cell faces f of the control volume Ω^{3h} . Averages needed to define the flux at the face between control volumes $\Omega_{i,j,k}^{3h}$ and $\Omega_{i+3,j,k}^{3h}$ are defined as

$$\bar{u}_f^{3h} = \frac{1}{2}(u_{i,j,k} + u_{i+3,j,k}), \quad (22a)$$

$$\widetilde{uv}_f^{3h} = \frac{1}{2}(u_{i,j,k}v_{i+3,j,k} + u_{i+3,j,k}v_{i,j,k}). \quad (22b)$$

The fourth-order scheme is constructed by annihilating the leading-order errors of the two second-order schemes. The cell volumes and the flux balances are both of order h^d . For the second-order schemes of equations (18) and (20), the leading-order error is therefore of order h^{d+2} . In particular, if the leading-order error is equal to Ch^{d+2} for the h scheme, then it is equal to $C(3h)^{d+2}$ for the $3h$ scheme, because the schemes use the same stencil. Applying Richardson extrapolation to annihilate the leading-order error results in the following finite-volume discretization of the gradient operator:

$$V_i \nabla_i F = B_i, \quad (23)$$

with

$$V_i = \frac{9}{8}V_i^h - \frac{1}{8 \cdot 3^d}V_i^{3h}, \quad (24a)$$

$$B_i = \frac{9}{8}B_i^h - \frac{1}{8 \cdot 3^d}B_i^{3h}. \quad (24b)$$

Since central differences are employed, the leading-order error is now of order h^{d+4} , i.e., a fourth-order scheme has been obtained. Note that the scheme is fourth-order accurate on non-uniform, curvilinear grids, provided that the mapping from the computational to the physical domain is sufficiently smooth.

A fourth-order discretization of the convective operator is obtained by applying the fourth-order discrete gradient operator, as defined above, in the definitions of the discrete skew-symmetric and symmetric operators as defined by equations (14) and (16). For the fourth-order scheme, conservation of both ϕ and ϕ^2 can be proven in the same manner as was done for the second-order scheme. This prove depends on the rules of equation (13). Because the fourth-order flux balance is a linear combination of the second-order flux balances, the fourth-order discrete gradient operator will satisfy these rules as well.

5 Dispersion-relation preserving scheme on curvilinear grids

In aeroacoustic applications, waves have to travel over long distances, which requires that the numerical scheme has low dissipation and dispersion. Dissipation is minimized by using central

differences and explicitly adding a minimal amount of artificial diffusion if required for stability. To minimize dispersion, the ideas of Tam & Webb (Ref. 7) are followed. Their dispersion-relation preserving (DRP) scheme uses finite differencing to discretize the gradient operator. A symmetric, seven-point stencil is used. The coefficients of the stencil have three degrees of freedom of which two are used to make the scheme fourth-order accurate and the remaining one is used to minimize the dispersion.

Thus, to apply the DRP approach to the fourth-order finite-volume scheme as presented in the previous section, an additional degree of freedom is needed. At each cell centre, a third control volume Ω_i^{2h} is introduced with a mesh size of $2h$ in the computational domain. Again, the same discretization stencil is employed on the $2h$ grid for the gradient operator, which can be written as

$$V_i^{2h} \nabla_i F = B_i^{2h}, \quad (25)$$

with V_i^{2h} the volume of the control volume Ω_i^{2h} and with B_i^{2h} the flux balance. Combining all three discretization stencils through Richardson extrapolation to annihilate the leading-order error, results in the following fourth-order finite-volume discretization of the gradient operator:

$$V_i \nabla_i F = B_i, \quad (26)$$

with

$$V_i = \beta \left(\frac{4}{3} V_i^h - \frac{1}{3 \cdot 2^d} V_i^{2h} \right) + (1 - \beta) \left(\frac{9}{8} V_i^h - \frac{1}{8 \cdot 3^d} V_i^{3h} \right), \quad (27a)$$

$$B_i = \beta \left(\frac{4}{3} B_i^h - \frac{1}{3 \cdot 2^d} B_i^{2h} \right) + (1 - \beta) \left(\frac{9}{8} B_i^h - \frac{1}{8 \cdot 3^d} B_i^{3h} \right). \quad (27b)$$

The parameter β leaves the necessary freedom to minimize the dispersion.

On a uniform grid, the finite-volume scheme can be written as a finite-differencing scheme. The value of the parameter β can be chosen such that, in that case, the finite-volume scheme is equivalent to the DRP scheme. On a uniform grid in one dimension, the finite-volume scheme reduces to the following symmetric finite-differencing scheme:

$$B_i = a_1 (F_{i+1} - F_{i-1}) + a_2 (F_{i+2} - F_{i-2}) + a_3 (F_{i+3} - F_{i-3}), \quad (28)$$

with the coefficients given by

$$a_1 = \frac{27 + 5\beta}{48}, \quad a_2 = -\frac{\beta}{12}, \quad a_3 = \frac{\beta - 1}{48}. \quad (29)$$

On a uniform grid in multiple dimensions, the finite-volume scheme reduces to this stencil for each computational direction separately. For the DRP scheme the coefficients are given by

$$a_1 = 0.770882380518, \quad a_2 = -0.166705904415, \quad a_3 = 0.0208431427703. \quad (30)$$

Using Taylor series expansions, it can be shown that the finite-differencing scheme is fourth-order accurate if the coefficients satisfy the following two relations:

$$a_1 + 2 a_2 + 3 a_3 = \frac{1}{2}, \quad (31a)$$

$$a_1 + 2^3 a_2 + 3^3 a_3 = 0. \quad (31b)$$

The coefficients of the finite-volume scheme and those of the DRP scheme satisfy these two relations. Thus, if one coefficient is made equal, then the other two must be equal as well and therefore the finite-volume scheme is made equivalent to the DRP scheme (on a uniform grid) by taking the value of β as

$$\beta = -12a_2 = 2.00047085298. \quad (32)$$

Note that the vertices of the control volume Ω^{2h} do not lie at grid points, but at cell centres. To compute the volume and the area vectors of this control volume, the coordinates of the cell centres are therefore required. To maintain the fourth-order accuracy of the scheme, these coordinates must be computed with fourth-order accuracy as well.

6 Propagation of an acoustic pulse

To illustrate that the proposed fourth-order finite-volume scheme has low numerical dispersion, even on non-uniform curvilinear grids, the propagation of a 2D acoustic pulse is considered. The linearized Euler equations (LEE) are solved. The steady flow is a uniform flow in positive x direction at a Mach number $M = 0.5$. Let ρ be the density, \mathbf{u} the velocity, p the pressure, and c the speed of sound, and let $'$ indicate the perturbation of a variable. The initial solution for the LEE equations is given by

$$\frac{\rho'}{\rho} = \frac{p'}{\gamma p} = A 2^{-(\|\mathbf{x}\|/b)^2}, \quad \mathbf{u}' = 0, \quad (33)$$

with amplitude $A = 0.01$ and half-width $b = 3L$ and with γ the ratio of specific heats. The flow domain is defined as $\mathbf{x} \in [-100L, 100L]^2$ with periodic boundary conditions.

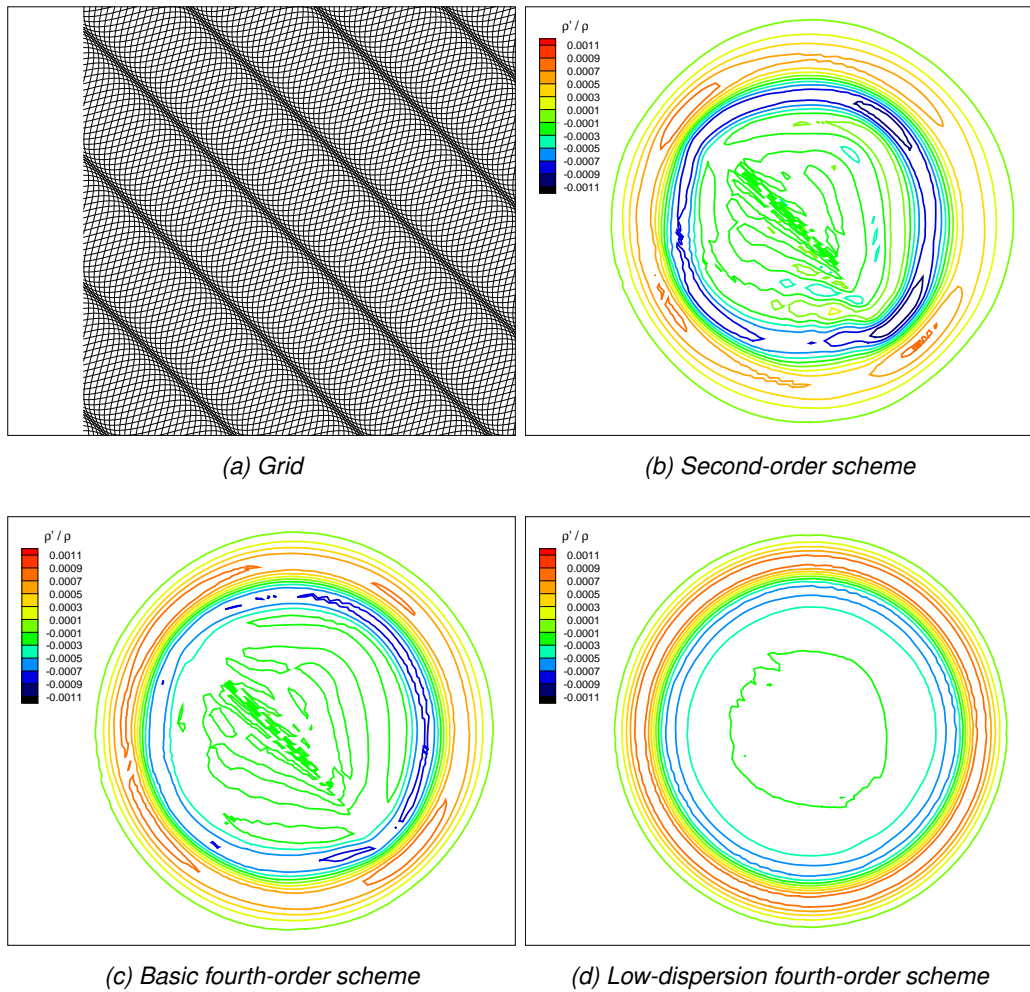


Fig. 2 Numerical solution of 2D acoustic pulse at time $ct/L = 32$ on strongly non-uniform curvilinear grid with 200×200 grid cells

The LEE equations are solved using the second-order scheme, the basic fourth-order scheme, and the fourth-order low-dispersion scheme. The skew-symmetric form is not used. The equations are integrated in time by the standard four-stage Runge–Kutta scheme. The size of the time step is set such that the Courant number is equal to one.

A non-uniform, curvilinear grid is employed with strong stretching and skewness, as illustrated in figure 2a. The grid has been obtained by a smooth mapping of a uniform grid in the computational domain to the physical domain.

Figure 2 gives the contour lines of the pressure distribution on the grid with 200×200 grid cells (i.e., average mesh size $\langle \Delta x \rangle / L = 1$) at time $ct/L = 32$ (i.e., the pulse has travelled a distance

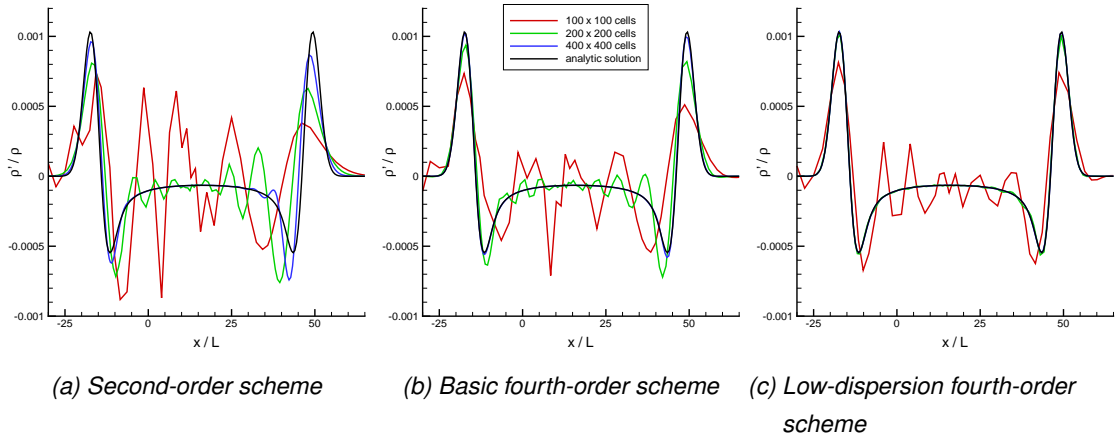


Fig. 3 Numerical solution of 2D acoustic pulse at time $ct/L = 32$ on strongly non-uniform curvilinear grid with varying number of grid cells compared to analytic solution at $y = 0$

of $32L$ in the direction normal to the flow velocity). For the second-order and basic fourth-order scheme, the non-uniformity of the grid has a strong effect on the contour lines, which become more and more distorted. For the low-dispersion fourth-order scheme, the circular shape of the contour lines are well maintained (only the innermost contour line is distorted, but there the solution is almost constant). The superiority of the low-dispersion scheme is also shown in figure 3 where the grid convergence is shown, compared to the exact solution. Note that all computations are stable without any explicit artificial diffusion.

7 Convection of an isentropic vortex

In order to test the capability of the high-order finite-volume scheme to accurately capture vortices without significant dissipation or dispersion, the convection of a 2D isentropic vortex in a uniform flow is considered, which is an exact solution of the compressible Euler equations. The uniform flow is in the positive x direction at a Mach number $M_\infty = 0.5$. The initial solution is given by

$$\mathbf{u} = \begin{pmatrix} u_\infty \\ 0 \end{pmatrix} + u_A e^{(1-(r/b)^2)/2} \begin{pmatrix} (y - y_0)/b \\ -(x - x_0)/b \end{pmatrix}, \quad (34)$$

and

$$\frac{T}{T_\infty} = \left(\frac{p}{p_\infty} \right)^{(\gamma-1)/\gamma} = \left(\frac{\rho}{\rho_\infty} \right)^{\gamma-1} = 1 - \frac{\gamma-1}{2} \frac{u_A^2}{c_\infty^2} e^{1-(r/b)^2}, \quad (35)$$

with T the temperature, with $r^2 = (x - x_0)^2 + (y - y_0)^2$ the distance from the vortex centre (x_0, y_0) , and with b the radius where the velocity induced by the vortex reaches its maximum value u_A . The flow domain is defined as $x \in [-100L, 100L]$ with periodic boundary conditions.

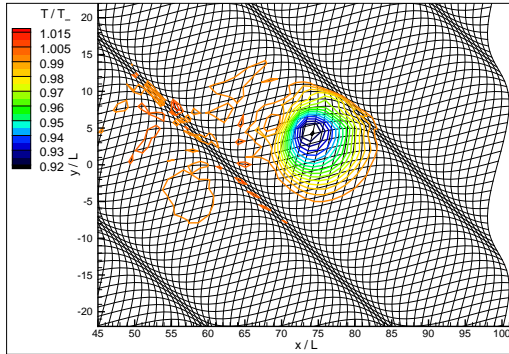
A strong, compact vortex is considered with $u_A/u_\infty = 0.8$ and $(b/L)^2 = 16/\ln 2$ (i.e., $e^{-(r/b)^2} = \frac{1}{2}$ at $r = 4L$). It is initially located at $(x_0, y_0) = (-75L, 0)$ and convected for a time period $u_\infty t/L = 150$. Computations are performed on the same strongly non-uniform grid as used for the acoustic pulse, with the number of cells ranging from 100×100 to 400×400 . The equations are integrated in time by a low-storage 4-stage Runge–Kutta scheme.

The second-order scheme, the basic fourth-order scheme and the low-dispersion fourth-order scheme are used. For all three schemes, computations using the skew-symmetric form of the convective operator are compared to computations based on the divergence form. The skew-symmetric form is stable without artificial diffusion. For the divergence form, standard flux averaging turned out to be unstable. Therefore, the fluxes at the cell faces are computed by averaging the flow variables per unit volume. This approach differs only slightly from the skew-symmetric form; in fact, for incompressible flow, it is equivalent to the skew-symmetric form.

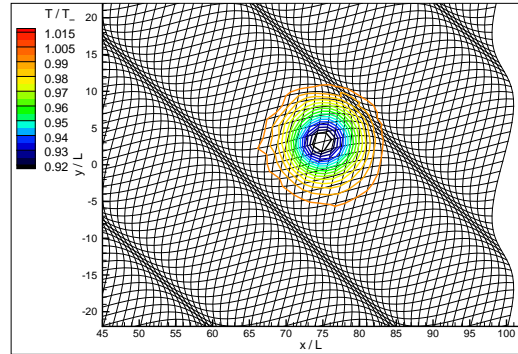
Figure 4 shows the temperature distributions on the medium grid (200×200 cells) computed with all six schemes. For the second-order scheme, the vortex has clearly lost its shape, in particular when using the divergence form, while also the centre of the vortex has drifted to a positive y position (of approximately $y = 4L$). The low-dispersion fourth-order scheme is the most successful in maintaining the shape and position of the vortex.

Figure 5 gives the difference of the numerical solution with the analytical solution as a function of the grid resolution for all six schemes (with h the mesh size in the computational domain). This shows that the fourth-order schemes are indeed fourth-order accurate on this strongly non-uniform, curvilinear grid. For the low-dispersion scheme, the error is reduced by an order of magnitude compared to the basic fourth-order scheme.

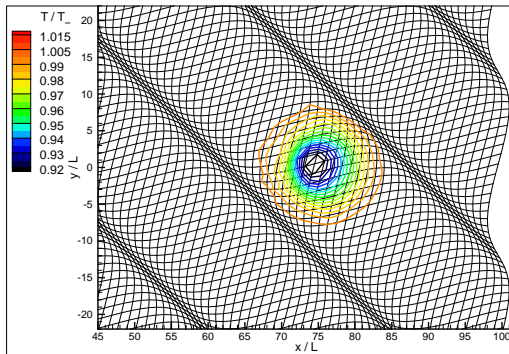
As the chosen approach for the divergence form differs only slightly from the skew-symmetric form, one would not expect large differences in the error levels. Indeed, the error levels for the velocity components are indiscernible. For the entropy, however, a clear reduction of the error by almost an order of magnitude is seen for the skew-symmetric form (figure 5d). Essentially, there is less entropy production using the skew-symmetric form, because it ensures that there is no dissipation (or creation) of kinetic energy stemming from the discretized convective operator. Larger differences would be expected with the divergence form based on averaging the fluxes, since it requires artificial diffusion to maintain stability.



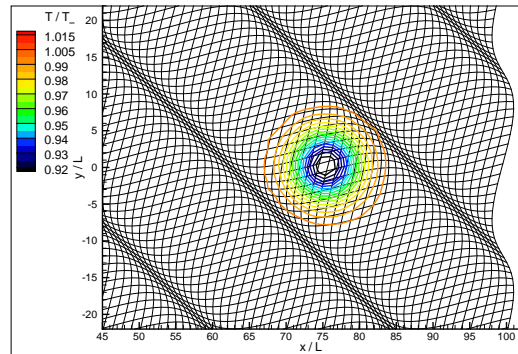
(a) Second-order scheme, divergence form



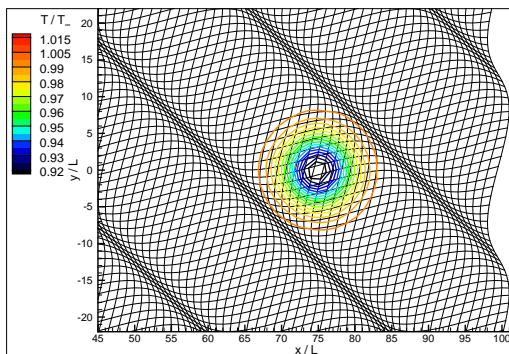
(b) Second-order scheme, skew-symmetric form



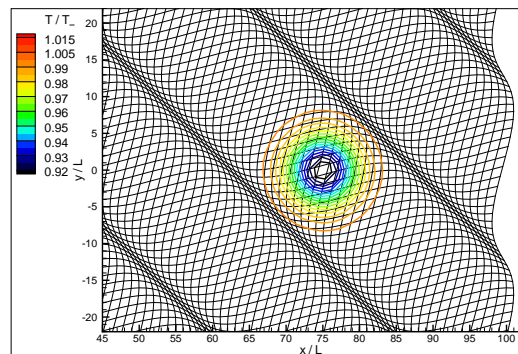
(c) Basic fourth-order scheme, divergence form



(d) Basic fourth-order scheme, skew-symmetric form



(e) Low-dispersion fourth-order scheme, divergence form



(f) Low-dispersion fourth-order scheme, skew-symmetric form

Fig. 4 Convection of strong isentropic vortex on strongly non-uniform grid: temperature field at time $u_\infty t/L = 150$ (centre should be located at $(x, y) = (75L, 0)$) on medium grid (200×200 cells)

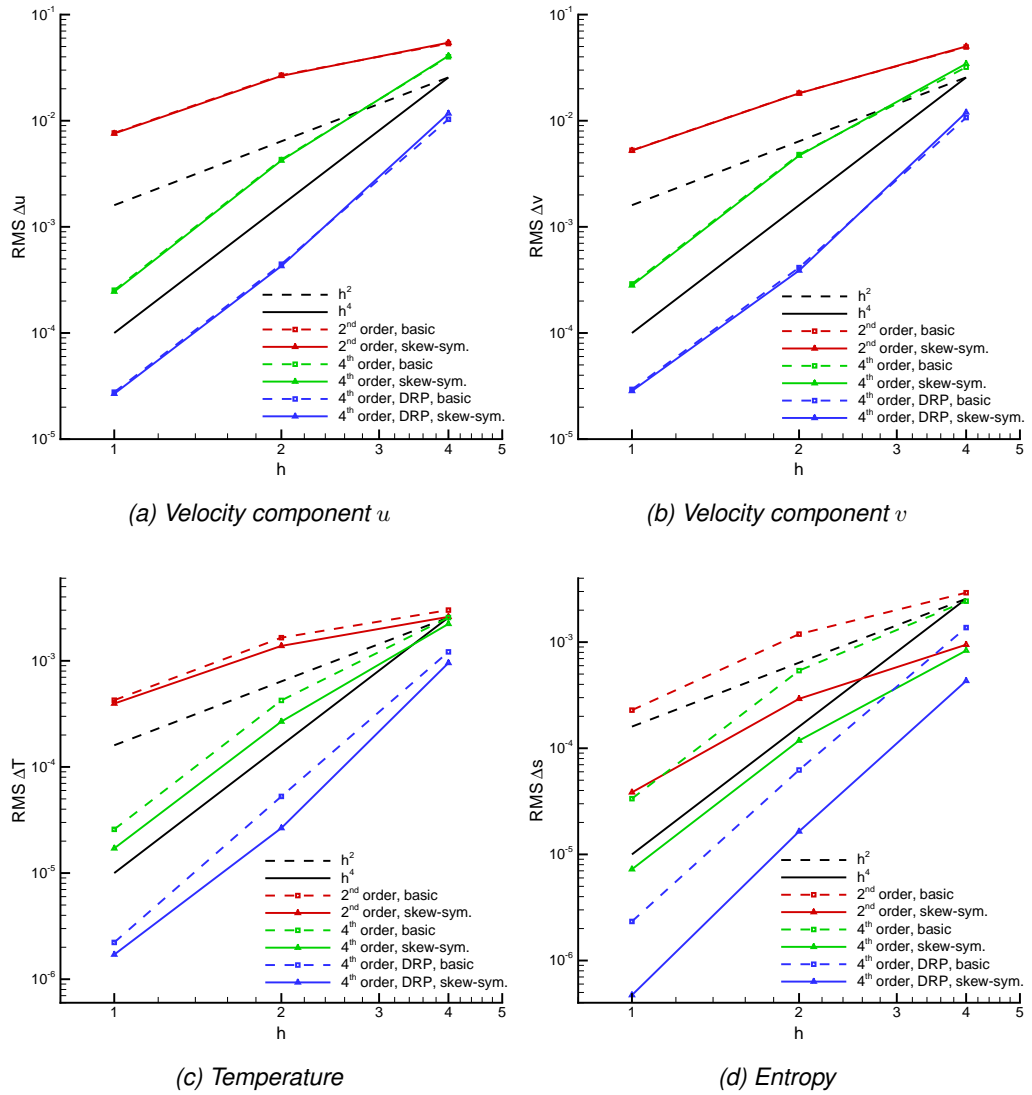


Fig. 5 Convection of strong isentropic vortex on strongly non-uniform grid: Grid dependence of root-mean-square value of difference with analytical solution at time $u_\infty t/L = 150$

8 Decaying isotropic homogeneous turbulence

The high-order finite-volume scheme is intended to be used for the X-LES model when in LES mode. To assess the numerical scheme in pure LES mode, the decay of isotropic homogeneous turbulence is considered. The results are compared to the experiment of Comte-Bellot and Corrsin (Ref. 1). In this experiment, the turbulence was generated by a grid with mesh size $M = 5.08$ cm and with an onset velocity of $U_0 = 10$ m/s. The Reynolds number based on these scales is $Re_0 = U_0 M / \nu = 34\,000$. In the computations, a cubic box of thickness $L = 10M$ is used with periodic boundary conditions. The initial solution consists of a random velocity field generated from the filtered experimental energy spectrum at time $t^+ = tU_0/M = 42$.

X-LES computations with the second-order scheme have been presented before by Kok et al. (Ref. 4). The same computational procedure is followed here. To study the grid dependence of the numerical scheme, a fixed filter width $\Delta = L/32$ is employed, while the mesh size is varied from $h = L/32$ to $h = L/128$. Because LES computes a filtered velocity field, the experimental data is filtered as well to allow a proper comparison (see again Kok et al. (Ref. 4) for details).

For compressible flow, the skew-symmetric form ensures that the kinetic energy is conserved by the convective operator. This is illustrated by first performing inviscid computations at compressible flow conditions (Mach number $M = 0.2$ based on the initial turbulence intensity $u_1 = 0.222$ m/s). Without viscous dissipation, the total kinetic energy in the box can only change due to the work done by the pressure. Figure 6 gives the time dependence of the total kinetic energy for computations on the coarse grid ($h = L/32$) with the skew-symmetric form and the divergence form (using flux averaging) and without artificial diffusion. The low-storage 4-stage Runge–Kutta scheme has been used with a small time step ($\Delta t^+ = 0.873$ or $u_1 \Delta t / h = 0.062$). The computation with the divergence form is unstable and breaks down within a short time period. For the computation with the skew-symmetric form, the kinetic energy also grows, but on a much larger time scale and at a rate that is negligible compared to the experimental decay (about 80% at time $t^+ = 170$). Thus, the skew-symmetric form strongly enhances stability and ensures that there is no significant dissipation or production of kinetic energy originating from the inviscid terms in the momentum equation. Therefore, no interference with the sub-grid scale model is expected for the X-LES computations.

Next, the grid convergence is considered for X-LES computations in pure LES mode at incompressible flow conditions. The equations are integrated in time by a second-order implicit scheme with time step $\Delta t^+ = 3.49$. Figure 7 shows the grid dependence of the energy spectra at times $t^+ = 98$ and $t^+ = 171$ for the second-order scheme with fourth-order artificial diffusion and

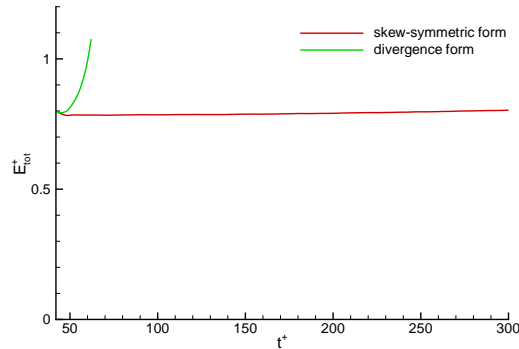


Fig. 6 Compressible isotropic homogeneous turbulence: time dependence of total kinetic energy for inviscid computations with low-dispersion fourth-order scheme using skew-symmetric and divergence forms and without artificial diffusion

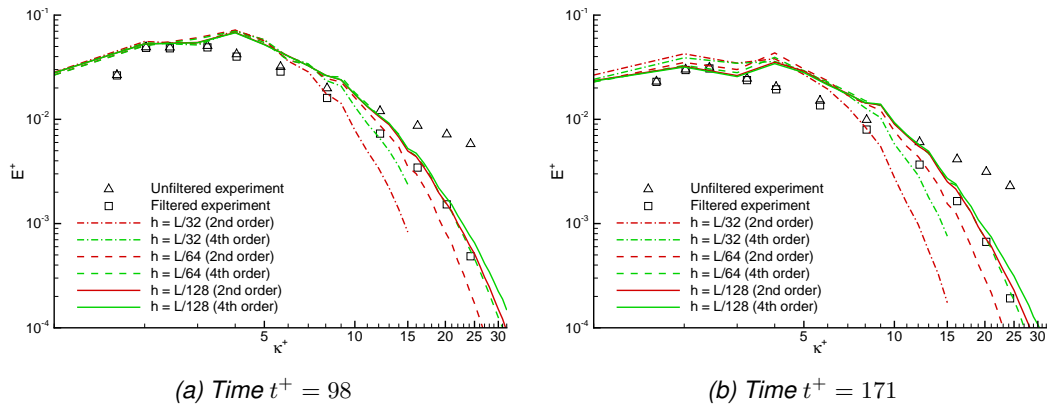


Fig. 7 Incompressible isotropic homogeneous turbulence: grid dependence of energy spectra for second-order and low-dispersion fourth-order schemes

the low-dispersion fourth-order scheme with sixth-order artificial diffusion. The fourth-order scheme has clearly improved the grid convergence over the second-order scheme. For sufficient accuracy, the second-order scheme requires at least a mesh size of $h = L/128$, i.e., four cells per filter width, while the fourth-order scheme obtains the same level of accuracy with a mesh size of $h = L/64$, i.e., two cells per filter width.

Finally, the effect of artificial diffusion is considered. Ideally, no artificial diffusion is used, but in practice it often is required to maintain stability. Figure 8 shows the decay of the total kinetic energy for the fourth-order low-dispersion scheme with and without sixth-order artificial diffusion. Both converge to the same solution for zero mesh size, but from opposite sides. With artificial diffusion, the grid convergence appears to be at least as good as it is without. The decay of kinetic energy is virtually grid independent at a mesh size $h = L/64$ (i.e., 2 cells per filter width). Thus, for this case, adding a limited amount of artificial diffusion appears to be harmless.

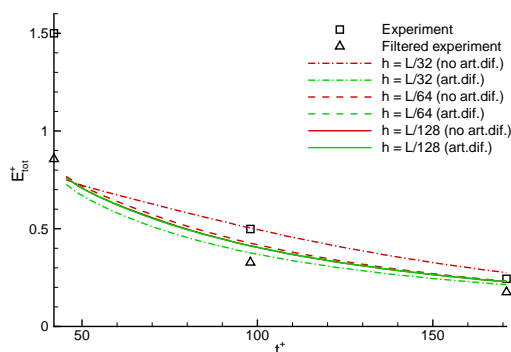


Fig. 8 Incompressible isotropic homogeneous turbulence: decay of total kinetic energy for low-dispersion fourth-order scheme with and without sixth-order artificial diffusion

9 Concluding remarks

A high-order finite-volume method has been presented that preserves both the symmetry properties and the dispersion relation of the convective operator. For X-LES computations of compressible flow, the discretization is based on the skew-symmetric form, which ensures that the kinetic energy is conserved by the convective operator. This enhances the numerical stability and minimizes the interference of numerical errors with the sub-grid scale model. The scheme has low numerical dissipation and dispersion which is essential to capture vortices accurately in X-LES computations and to allow sound waves to travel over long distances for aeroacoustic computations. Finally, it has been demonstrated that the scheme maintains these advantageous properties as well as its fourth-order accuracy on non-uniform (yet smooth) curvilinear grids.

Acknowledgements

This work was partially performed within the EU project DESider (Detached Eddy Simulation for Industrial Aerodynamics), which is funded by the European Union under Contract No. AST3-CT-2003-502842 of the European Commission, and as part of NLR's Basic Research Programme.

The author would like to thank Prof. Arthur Veldman for fruitful discussions on skew symmetry and high-order schemes.

References

1. G. Comte-Bellot and S. Corrsin. The use of a contraction to improve isotropy of grid generated turbulence. *Journal of Fluid Mechanics*, 25:657–682, 1966.
2. W.J. Feiereisen, W.C. Reynolds, and J.H. Ferziger. Numerical simulation of a compressible, homogeneous, turbulent shear flow. Report TF-13, Thermosciences Division, Mechanical Engineering, Stanford University, 1981.
3. A.E. Honein and P. Moin. Higher entropy conservation and numerical stability of compressible turbulence simulations. *Journal of Computational Physics*, 201(2):531–545, 2004.
4. J.C. Kok, H.S. Dol, B. Oskam, and H. van der Ven. Extra-large eddy simulation of massively separated flows. In *42nd AIAA Aerospace Sciences Meeting*, Reno, NV, 5–8 January 2004. AIAA paper 2004-264.
5. J.C. Kok and S.P. Spekreijse. Efficient and accurate implementation of the k - ω turbulence model in the NLR multi-block Navier–Stokes system. In *ECCOMAS 2000*, Barcelona, Spain, 11–14 September 2000.
6. A. G. Kravchenko and P. Moin. On the effect of numerical errors in large eddy simulations of turbulent flows. *Journal of Computational Physics*, 131:310–322, 1997.
7. C.K.W. Tam and J.C. Webb. Dispersion-relation-preserving finite difference schemes for computational acoustics. *Journal of Computational Physics*, 107:262–281, 1993.
8. R.W.C.P. Verstappen and A.E.P. Veldman. Symmetry-preserving discretization of turbulent flow. *Journal of Computational Physics*, 187(1):343–368, 2003.
9. R.W.C.P. Verstappen and A.E.P. Veldman. Symmetry-preserving discretizations of the incompressible Navier-Stokes equations. In P. Wesseling, E. Oñate, and J. Périaux, editors, *ECCOMAS CFD 2006*, Egmond aan Zee, The Netherlands, 5–8 September 2006.